provides an ideal environment for β-elimination. This reaction appears to compete effectively with decarbonylation so that only small ketones react in the latter way. Larger straight-chain aliphatic ketones undergo extensive dehydrogenation while ketones branched at the α carbon prefer to eliminate methane. Whether or not this generalization may be extended to ketones containing secondary or tertiary β carbons still remains to be tested.

Acknowledgment is made to the donors of the Petroleum Research Fund, administered by the American Chemical Society, and to the Department of Energy (DE-AC02-80ER10689). The authors also wish to express their appreciation to Dr. J. Kouba for his helpful discussions.

Photoprocesses in Cationic Microemulsion Systems[1]

S. S. Atik and J. K. Thomas*

Contribution from the Chemistry Department, University of Notre Dame, Notre Dame, Indiana 46556. *Received January 30, 1981*

Abstract: Photophysical methods are used to investigate the hexanol, dodecane, water, and cetyltrimethylammonium bromide (CTAB) microemulsion (μE), both as oil in water and water in oil systems. Several photochemical systems, e.g., the pyrene excimer formation, the pyrene–dimethylaniline exciplex and electron transfer system, and the ruthenium bipyridyl–methyl viologen electron system, are used to determine the particle radii and surfactant aggregation number. Fluorescence methods are used to investigate the site and environment of reactants in these systems. The effects of emulsion parameters, e.g., water content, nature of surface, etc., on electron-transfer reactions are studied and discussed.

There has been extensive photochemical studies on micellar systems and in particular CTAB.[2,3] As an extension of this work, we chose the CTAB-μE system (oil in water (O/W) and water in oil (W/O) for our present investigation. The objective of such an undertaking is to explore the influence of these structurally different molecular assemblies of the same surfactant molecule (CTAB) on a variety of photochemical and photophysical processes. A useful byproduct of this study is the elucidation of the fundamental basic structure of the host micellar or μE particles and water pools and the nature of their interaction with solutes.

Experimental Section

Fluorescence spectra were measured on a Perkin–Elmer MPF 44 spectrofluorimeter. Laser flash photolysis studies were carried out with the use of a Korad KIQ frequency doubled Q switch ruby laser: with 3471 Å; pulse width, 15 ns; and energy, 0.1 J. The transitory signals developed by the laser pulse were monitored on a Tektronix 7912AD transient capture device, while data processing was carried out on a Tektronix 4051 computer.

All chemicals were obtained from sources indicated previously, where the purification methods were also outlined.[4-6]

Results and Discussion

The results of this study will be described in two sections, the first one dealing with (O/W) CTAB-μE and the second one with W/O μE, where μE is an abbreviation for microemulsion.

Oil in Water (O/W) CTAB-μE. These μE particles are composed of CTAB, hexanol, and dodecane stabilized in an aqueous medium. These aggregate assemblies which are often referred to as swollen micelles are believed to consist of an oil droplet center coated with a mixed monolayer of surfactant and co-surfactant (hexanol) molecules with their ionic or polar groups directed outward in contact with the aqueous phase. The photochemical and photophysical studies presented in this paper are found to be consistent with this description.

The μE System. The composition of the μE used in this endeavor consisted of 8.37% CTAB, 0.5% hexanol, and 1.0% oil (dodecane) in water (or 0.01 M CTAB, 0.05 M hexanol, and 0.06 M dodecane). The solution formed from these components was very slightly bluish (light scattering) but otherwise perfectly clear. A useful ternary phase diagram for CTAB, hexanol, and water has already been reported by Friberg.[7]

Oil in Water (O/W) μE Size Determination. The average size of the μE particle was determined by the time-resolved pyrene excimer formation technique recently described by one of the authors.[8] The method relies on the assumption that solutes are distributed among the μE partilces according to Poisson statistics. According to this method the time-resolved fluorescence intensity is given by,

$$I_F(t) = I_F(0)e^{-\{k_1 t + \bar{n}(1-e^{-k_e t})\}} \quad (1)$$

where $I_F(t)$ and $I_F(0)$ are the fluorescence intensities of excited pyrene at time t and $t = 0$, respectively, $\bar{n}$ is the average pyrene occupancy of a μE particle given by $[P]/[\mu E]$, k_e is a first-order intra-μE excimer formation rate constant for a particle containing two pyrene molecules one of which is in its excited singlet state, and finally k_1 is the first-order rate of decay of P* solubilized in a particle that does not contain other pyrene molecules (i.e., the lifetime of P* under conditions where no excimer emission is observed at $\bar{n} \leq 0.1$).

For a certain $\bar{n}$ value ($\bar{n} \geq 0.2$) where Poisson law ($\alpha_n = \bar{n}^n e^{-\bar{n}}/n!$, α_n is the probability of finding a μE particle containing n probe molecules) predicts the existence of μE particles with two or more solubilized pyrene molecules, the fluorescence decay curve shows two components (as predicted by eq 1)—an initial fast one attributed to μE particles having solubilized two or more P molecules, and a limiting slow one corresponding to particles that contain only one P molecule.

At sufficiently long times when all the fluorescence eminating from multiply occupied μE particles has decayed completely (i.e., $e^{-k_e t} = 0$) the remaining fluorescence intensity can be ascribed

(1) The authors would like to thank the NSF for support of this research via Grant CHE78-24867.
(2) J. K. Thomas, *Chem. Rev.*, **80**, 283 (1980).
(3) N. J. Turro, M. Grätzel, and A. M. Braun, *Angew. Chem.*, **19**, 675 (1980).
(4) M. Almgren, F. Grieser, and J. K. Thomas, *J. Am. Chem. Soc.*, **101**, 279 (1979).
(5) M. Almgren, F. Grieser, and J. K. Thomas, *J. Am. Chem. Soc.*, **102**, 188 (1980).
(6) S. Gregoritch and J. K. Thomas, *J. Phys. Chem.*, **84**, 149 (1980).
(7) S. Ahmad and S. Friberg, *J. Am. Chem. Soc.*, **94**, 5196 (1972).
(8) S. S. Atik and L. A. Singer, *Chem. Phys. Lett.*, **59**, 519 (1978); **66**, 234 (1979).

0002-7863/81/1503-4367$01.25/0

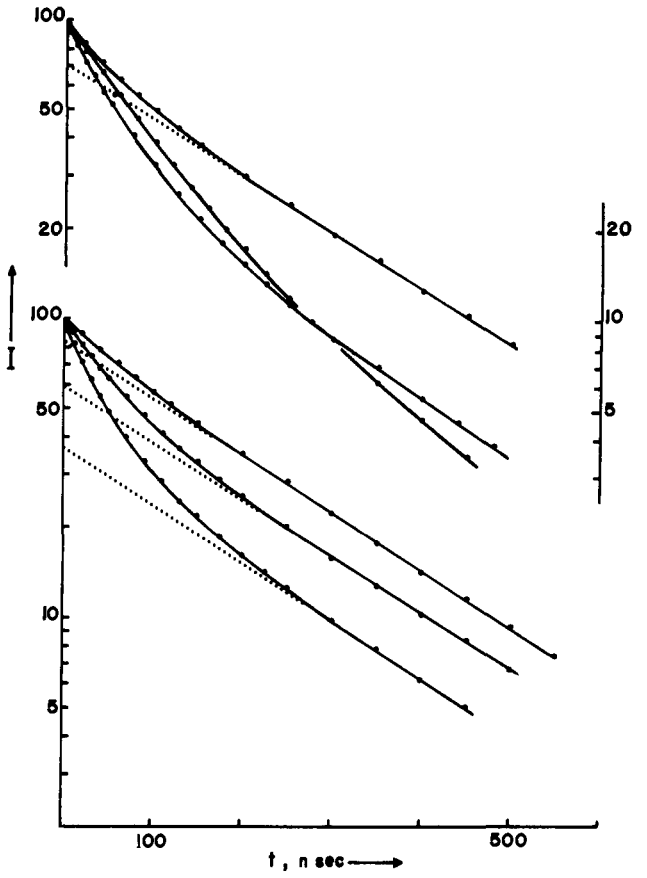

Figure 1. Rate of decay of pyrene fluorescence, I, at various [pyrene] and conditions (curves numbered from top to bottom): 1, [pyrene] = 1.0×10^{-4} M (CTAB); 2, [pyrene] = 1.0×10^{-4} M (0.01 M CTAB + 0.05 M hexanol); 3, [pyrene] = 1.0×10^{-4} M (CTAB microemulsion); 4, [pyrene] = 5.0×10^{-5} M (0.01 M CTAB + 0.05 M hexanol); 5, [pyrene] = 1.5×10^{-4} M (0.01 M CTAB + 0.05 M hexanol); and 6, [pyrene] = 3.0×10^{-4} M (0.01 CTAB M + 0.05 M hexanol).

to the unquenched P of singly occupied particles and will be given by,

$$I_F(t) = I_F(0)e^{-(\bar{n}+k_1)t} \quad (2)$$

Therefore, the limiting linear slope of the log plot of $I_F(t)$ vs. t will be given by $(-k_1)$ and the extrapolated intercept will be equal to $(-\bar{n})$. From this experimentally determined value of $\bar{n}$ and the molar concentration of P, the concentration of μE partilces in solution can be calculated.

It is important to note here that the described case is not always realized and can only be observed for systems where $k_e \gg k_1$. In cases where k_e is comparable to k_1 the fluorescence decay will no longer exhibit two distinct components since the contribution of excimer fluorescence to the total fluorescence intensity from multiply occupied particles will always be significant even at very long times $t \gg 1/k_1$. Nonetheless in such cases the observed nonexponential fluorescence decay can be fitted to eq 1 by a two-parameter ($\bar{n}$ and k_e) computer program and therefore an estimate of $\bar{n}$ can still be achieved.

Examples of the two cases discussed above are given in Figure 1. Note that the continuously nonexponential fluorescence decay is actually observed for the CTAB micelle. However, upon addition of hexanol the decay exhibits two easily discernible components resulting from an increase in the rate of excimer formation (k_e) which may be associated with an increase in the microfluidity of the mixed micelle. The two-component fluorescence decay is also noted for the μE particle. The solid curves in Figure 1 show the best-fit simulations according to eq 1. The results of such a time-resolved fluorescence-decay analysis are detailed in Table I.

The surfactant aggregation number (N) for the various molecular assemblies is calculated from the derived values of $\bar{n}$ which may be expressed as $(N[P]/([CTAB] - CMC))$, using the literature CMC value of 9.6×10^{-4} M for the micelle and the estimated value of 5.0×10^{-4} M for the CTAB–hexanol mixed micelle and for the μE particle. Under our experimental condition of [CTAB] $\gg$ CMC the calculated values of N should not be affected by errors in the approximated values of the CMC.

Table I also shows the numbers of hexanol and dodecane molecules per aggregate which were calculated based on the assumption that they are completely incorporated into the aggregates. Such an assumption is justified since neither hexanol nor dodecane are soluble in water. Simple calculations utilizing the density of dodecane and the concentration of the μE particles in solution yield a radius of 40 Å for the oil droplet.

Table I. Kinetic Parameters Obtained from Intra-Aggregate Excimer Fluorescence Quenching Decay Analysis

[P], M	$\bar{n}$	$k_1 \times 10^{-6}$, s^{-1}	$k_e \times 10^{-7}$, s^{-1}	N CTAB	N hexanol	N dodecane
		0.01 M CTAB				
5.0×10^{-5}	0.40	5.88	0.50	75		
1.0×10^{-4}	0.82	5.85	0.60			
		0.01 M CATB + 0.05 M Hexanol				
5.0×10^{-5}	0.17	4.35	1.30	33	170	
1.5×10^{-4}	0.53	4.30	1.40			
3.0×10^{-4}	1.00	4.40	1.35			
		CTAB-μE (O/W)				
1.0×10^{-4}	1.35	4.00	0.80	135	670	800

Table II. Physical Parameters Obtained from Fluorescence Experiments at Room Temperature (22 °C)

	III/I	τ, ns N_2	τ, ns air	$[O_2] \times 10^3$,[a] M	$k_q(I^-) \times 10^{10}$, M^{-1} s^{-1}/N_2
		5.0×10^{-6} M PSA(K)			
0.01 M CTAB		50	44	0.27	13
0.01 M CTAB + 0.05 M hexanol		65	50	0.46	9.3
CTAB-μE (O/W)		70	40	1.00	7.9
		5.0×10^{-6} M P			
0.01 M CTAB	0.77	170	120	0.25	5.2
0.01 M CTAB + 0.05 M hexanol	0.88	230	115	0.44	1.60
CTAB-μE (O/W)	1.14	260	43	1.90	0.72
dodecane + hexanol (2:1 (v/v))	1.30				

[a] Calculated from the relationship $1/\tau_{air} = 1/\tau_{N_2} + k_q[O_2]$ and taking $k_q = 10^{10}$ M^{-1} s^{-1}.

Table III. Fluorescence Quenching Data of 5.0×10^{-5} M P or P Derivatives at 0.02 M Quencher in CTAB-μE ($W_o = 20.3$) at Room Temperature (22 °C)

	τ_F^0, ns N_2	τ_F^0, ns air	$[O_2] \times 10^3$,[a] M	$k_q \times 10^{-9}$, M^{-1} s^{-1} DMA	MDA	CPC	I^-
P	380	22	4.2	2.7	2.0	0.42	0.40
PSA	65	35	1.2	2.3	0.8	5.3	7.4
PBA	195	41	2.0	2.0	0.8	2.1	0.75
PDA	200	28	3.1	2.0	0.85	1.0	0.50

[a] Calculated by using the fluorescence lifetimes under N_2 bubbled and nondegassed conditions and assuming $k_q(O_2) = 10^{10}$ M^{-1} s^{-1}.

Fluorescence Quenching and Laser Flash Photolysis Experiments

Site of Solubilization of P. The pyrene fluorescence spectrum has been shown to be extremely sensitive to the polarity of the local environment. Table II shows the variation in the ratio of two characteristic fluorescence band intensities (III/I) (a pa-

rameter which has been found to be a measure of the hydrophobicity of pyrene microenvironment)[9] for the different molecular aggregates of CTAB described above. This table also includes O_2 concentrations sensed by potassium pyrene sulfonate, PSA(K), and pyrene, which are expected to be located in two different regions of the micelle or the μE particle, and their accessibility to quenching by I^- which would be partially bound to the surface of the various micellar aggregates but in fast exchange with the aqueous phase.

The increase in the III/I value when hexanol is added to the CTAB micelle seems to suggest that pyrene which resides close to the Stern layer of the micelle is pushed by hexanol to a more hydrophobic site closer to the micelle core. The further increase in the observed value of III/I in the O/W μE system appears also to indicate the solubilization site of pyrene to be in the oil droplet of the μE particle. This interpretation is consistent with the results of the quenching of P* by O_2 and I^- displayed in Table II. This is also substantiated by the increase in the microfluidity of the pyrene environment in going from CTAB micelles to CTAB microemulsions as measured by the intra-aggregate excimer formation rate constant (k_e) in Table I. The much smaller decrease in the quenching rate of excited PSA by I^- on going from micelle to microemulsion is attributed to a concomitant decrease in the binding of I^- to the aggregate structure.

Photoinduced Electron-Transfer Reactions. Laser flash photolysis studies of photoinduced electron-transfer (ET) processes are used to investigate the yield and stability of the laser-produced radical ions. Systems investigated include the well-established ET from dimethylaniline (DMA) to the laser produced excited singlet state of pyrene (P) and P derivatives, pyrenetetrasulfonic acid (PTS), pyrenesulfonic acid (PSA), pyrenebutyric acid (PBA), and pyrenedodecanoic acid (PDA),[10] as potassium salts.

Under conditions of >95% quenching of excited pyrene, P*, the yield of pyrene anion radical (monitored at 493 nm) was found to decrease substantially (50%) when hexanol was added to the CTAB micelle (where ion separation was found to be very efficient) and show a further dramatic decrease (85%) in the O/W μE system. Such an observation may be explained by the observed increase in the hydrophobicity of the pyrene environment as discussed above. It is important to note here that P/DMA exciplex emission was extremely weak in all three cases.

On the other hand, the decrease in the observed yield of the pyrenyl anion of PTS, PSA, PBA, and PDA was much less significant (<25%) in the various aggregate structures. The solubilization site of these pyrenyl derivatives remains close to the Stern-layer region of the micellar or μE particle where ET reactions and probability of escape of the produced ions appears to be most favorable.

Photochemical Studies in W/O μE System. Water in oil (W/O) μEs are apparently homogeneous and transparent systems containing small spherical water droplets (10–100 Å) surrounded by a mixed film of surfactant and co-surfactant (short-chain alcohol) molecules dispersed in a continuous medium of oil (hydrocarbon liquid). The particular system chosen for our studies consists of water–dodecane–CTAB–hexanol. Since this system has not been investigated previously, we shall describe first how the system was characterized and some important physical parameters (such as water core radius and composition of the water–hydrocarbon interface) obtained.

The W/O μE is prepared by titrating a mixture of water (1–3 mL), 1.0 g of CTAB, and 20.0 mL of dodecane with (2.0–2.5 mL) hexanol until a perfectly clear solution *is* obtained. An important parameter that determines the size of the water pool is the molar ratio of water to surfactant (W_0 = [H_2O]/[CTAB]). A fluorescence quenching technique that has been successfully applied to micelles is used to determine the size of the water pool (WP) as a function of W_0.

(9) K. Kalyanasundaram and J. K. Thomas, *J. Am. Chem. Soc.*, 99, 2039 (1977).

(10) B. Razan, M. Wong, and J. K. Thomas, *J. Am. Chem. Soc.*, **100**, 1679 (1978).

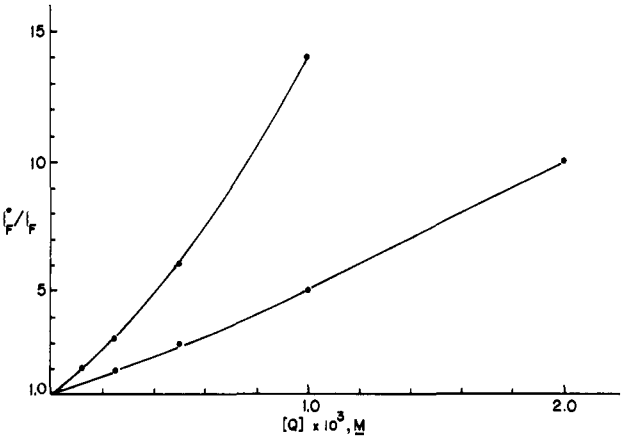

Figure 2. Variation in the ratio of the luminescence intensity without quencher to that with quencher, I_F°/I_F, with [quencher] in CTAB, microemulsion, W_0 = 40.5 (10% H_2O); [RuII] = 5.0 × 10^{-5} M: upper curve, methyl viologen, MV^{2+}; lower curve, heptyl viologen, HV^{2+}.

The fluorescence quenching method is based on the Poisson statistical distribution of quenchers among the water pools. The luminescent probe used is tris(bipyridyl)ruthenium(II) [RuII], and the quencher chosen is methylviologen (MV^{2+}); both salts were chlorides and both of these reactants are exclusively solubilized in the water pools. The existence of water pools in the system in which RuII and MV^{2+} are statistically distributed is confirmed[11] by the observed upward curvature in the Stern–Volmer plot (Figure 2) which can be described by the relationship,

$$\frac{I_F}{I_F^0} = \sum_{n=0}^{\infty} \frac{\alpha_n}{1 + n(k_q/k_1)} \tag{3}$$

where I_F and I_F^0 are the luminescence yields of RuII in the presence and absence of MV^{2+}, respectively, and α_n is the Poisson probability for the existence of a water pool that contains n quenchers and is given by $(\bar{n}^n e^{\bar{n}}/n!)$ where $\bar{n}$ = [MV^{2+}]/[WP], and k_1 is a first-order rate of decay of excited RuII in a water pool that does not contain any Q (equivalent to the luminescence lifetime of (RuII)* in the absence of Q).

The presence of water pools is further substantiated by the observed lower quenching efficiency of heptylviologen (HV^{2+}) as compared to MV^{2+} (Figure 2) which is due to its decreased mobility as a result of binding at the water–hydrocarbon interface.

The adjustable parameters in eq 3 are [WP] and k_q. The size of the water pool may be determined from the value of [WP] that produces the best fit to the experimental Stern–Volmer curve.

The luminescence decay of (RuII)* in the presence of MV^{2+} can also be analyzed according to eq 1. In this case $\bar{n}$ would be given by [MV^{2+}]/[WP]. Figure 3 gives the various types of decays observed with varying amounts of solubilized water (W_0). The solid curves are the best-fit simulations obtained by varying the adjustable parameters k_q and $\bar{n}$. The water pool concentration can then be determined from the derived values of $\bar{n}$ and the known total [MV^{2+}]. From the total amount of water in solution and the experimentally determined [WP], one can calculate the volume of the water pool and therefore the radius (assuming a spherically shaped water pool).

Results of the luminescence decay analysis are shown in Table IV. This table also includes other important parameters which are obtained from the experimentally determined [WP] such as the size of the water pool, the surfactant aggregation number, and the average surface area occupied by a surfactant molecule. Variations of these water pool parameters with the amount of solubilized water (W_0) are depicted in Figure 4.

The amount of hexanol present at the interface is determined by a known procedure. We fixed the amount of CTAB (1.0 g) and water (1.0 mL) in the system and tried different values for

(11) S. S. Atik and J. K. Thomas, *J. Am. Chem. Soc.*, in press.

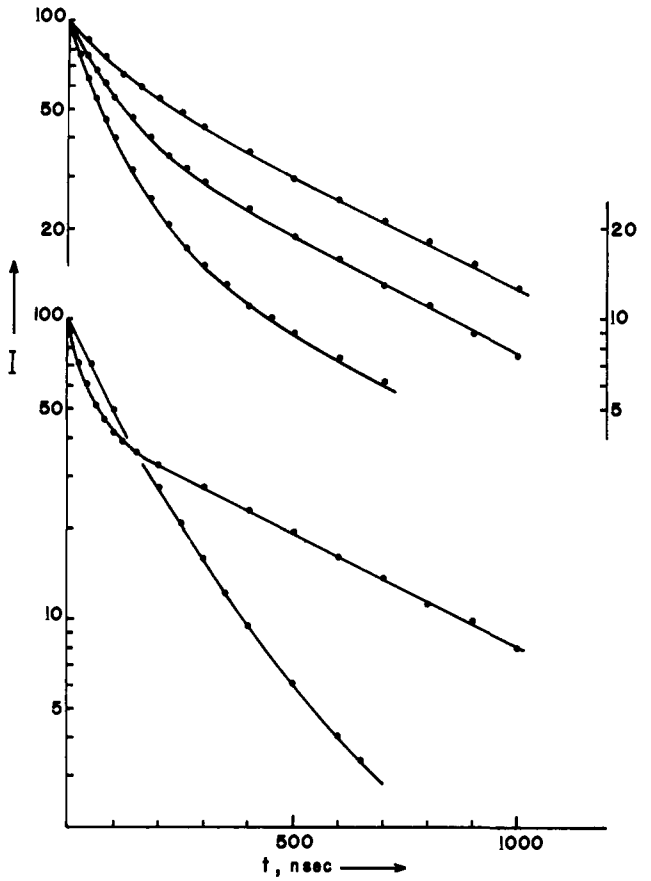

Figure 3. Variation in intensity of RuII* luminescence with time. [RuII] = 2.0×10^{-5} M. Curves 1 to 5 from top: 1, $[MV^{2+}] = 1.0 \times 10^{-4}$ M, $W_0 = 40.6$; 2, $[MV^{2+}]$ 2.0×10^{-4} M, $W_0 = 40.6$; 3, $[MV^{2+}]$ 4.0×10^{-4} M, $W_0 = 40.6$; 4, $[MV^{2+}]$ 5.0×10^{-4} M, $W_0 = 20.3$; and 5, $[MV^{2+}]$ 5.0×10^{-4} M, $W_0 = 60.9$.

Table IV. Experimental Parameters Derived for the CTAB-(W/O) μE System (1.0 g CTAB, 2.0 mL of Hexanol and 20 mL of Dodecane) at 5.0×10^{-5} M Ru^{II} under Deaerated Ambient Conditions[a]

W_0	$[MV^{2+}] \times 10^4$	$\bar{n}$	$k_g \times 10^{-7}$, s^{-1}	$k_1 \times 10^{-6}$, s^{-1}	water $^1/_2$pp R_w, Å
20.3	5.0	0.80	2.0	1.75	32
40.6	1.0	0.38	0.70	1.70	54
	2.0	0.82	0.75	1.75	
	4.0	1.60	0.65	1.75	
60.9	5.0	3.70	0.15	1.72	81

W_0	N	a, Å^2
20.3	225	57
40.6	548	67
60.9	1250	66

[a] N, Aggregation no. of CTAB. a, area per head group of surfactant. R_w = radius of WP.

the W/O ratio. For each water–CTAB–dodecane mixture we measured the minimum amount of hexanol to be added to obtain a transparent solution. Figure 5 shows the plot of hexanol volume as a function of dodecane. Since the amount of CTAB present in the system is constant, the alcohol quantity should vary linearly with dodecane volume as is actually observed (Figure 5). Extrapolation of the linear plot in Figure 5 yields a Y intercept of 0.75 mL of hexanol which corresponds to the amount of hexanol associated with the water pools. It is thus estimated that for every CTAB surfactant molecule there are ca. 2.2 hexanol molecules adsorbed at the interface.

Fluorescence Quenching and Laser Flash Photolysis Studies. A fluorescence quenching technique is used to provide information regarding the solubilization site and the mode of interaction of

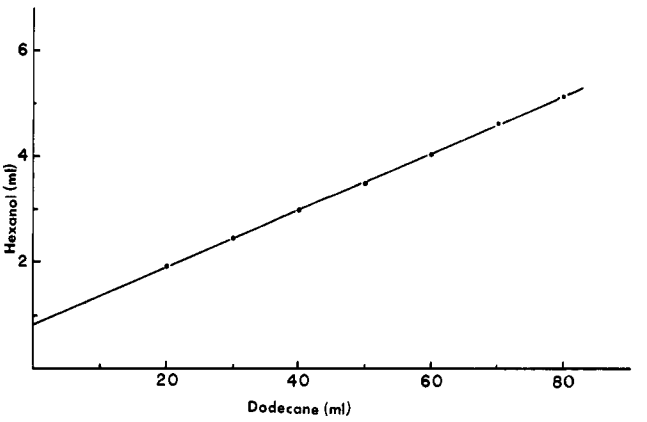

Figure 4. Titration with hexanol to clarity of a (W/O) μE containing 1.0 g of CTAB, 1.0 mL of water, and varying quantities of dodecane.

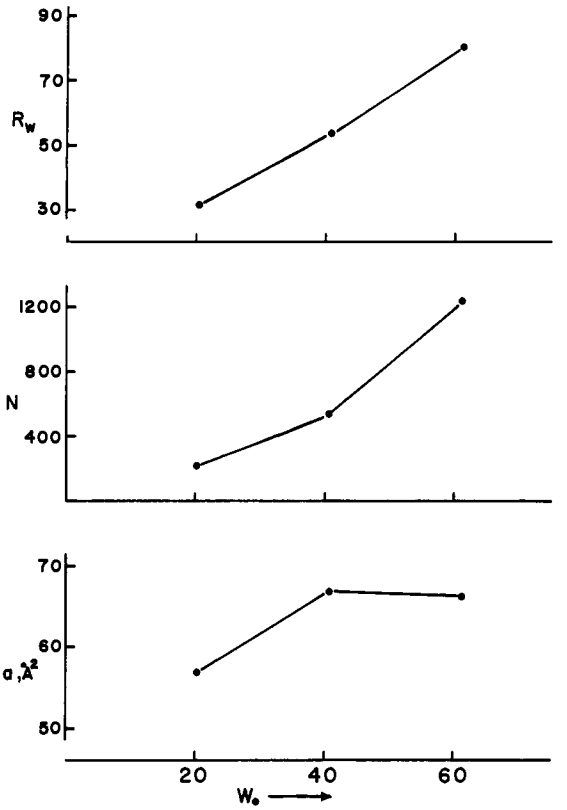

Figure 5. Physical properties of microemulsion as a function of W_0. Top: Raidus of water pool, R_w, in Å ($18[H_2O] = 10^{-24}N_0[WP]^4/_3\pi R_w^3$). Middle: Aggregation number of surfactant, N ($N = [CTAB]/[WP]$). Bottom: Area per surfactant head group, a ($a = 4\pi R_w^2$ Å^2).

solubilized molecules with the water pool structure of the CTAB-μE system. Laser excited P, PSA(K), PBA(K), and PDA(K) are quenched with various quenchers which are expected to exhibit different modes of interaction in the μE system. Typical quenchers used are DMA which probably has some affinity for the WP and also moves indiscriminately throughout the system, *N*-methyl-*N*-dodecylaniline (MDA)[12] which favors the hydrocarbon phase rather than the WP structure, cetylpyridinium chloride (CPC) which should be completely associated with the WP with the pyridinium quenching head group located at the interface in contact with water, and finally NaI which would be

(12) *N*-Methyl-*N*-dodecylaniline was made by refluxing for 12 h a mixture of 0.1 mol of *N*-methylaniline, 0.1 mol of dodecyl bromide, and 5 g of K_2CO_3 in 50 mL of methanol. The product was isolated by fractional distillation under vacuum and identified by NMR, and its purity was checked by gas chromatogrphic analysis (99% pure).

exclusively dissolved in the WP.

The results of the quenching experiments are given in Table III. These quenching data seem to indicate that P which resides in the hydrocarbon medium is more efficiently quenched by quenchers which partition strongly into the hydrocarbon phase. On the other hand, PBA and PDA which are strongly bound to the water pool structure with their carboxylate groups anchored at the interface strongly interacting with the trimethyl ammonium groups of the surfactant molecules are more strongly quenched than P by quenchers that are associated with the water pool aggregate. However, PSA which is likely to be associated with the head groups of the surfactant molecules in the Stern-layer region is most efficiently quenched by I^- and CPC which are localized within the WP structure.

Photoinduced ET Reactions. P/DMA. In the CTAB-μE system (W_0 = 20.3), DMA quenches efficiently the fluorescence of P as well as that of PSA, PBA, and PDA (Table III). This quenching leads to very weak exciplex emission (lifetime 60 ns) in the case of P whereas no exciplex emission is observed for the P derivatives. However in a mixture of dodecane and hexanol having the same composition as in the μE system, DMA quenching of the fluorescence of P as well as its derivatives produces a strong exciplex emission with a measured lifetime of 110 to 120 ns. The much shorter lifetime of the P/DMA exciplex in the μE system seems to indicate that it is strongly quenched by the water pools. On the other hand, PSA, PBA, and PDA are expected to be bound to the water pool structure and therefore the absence of exciplex emission can be ascribed to static quenching by the water pools.

Laser flash photolysis studies on pyrene and its derivatives showed a very low yield of P^-, but a very high yield of anions for the pyrenyl derivatives. This result is in accord with the explanation given earlier for the low yield of P^- in the O/W CTAB-μE system, i.e., that high yields of ions in photoinduced ET reactions can only be achieved when the reactants are solubilized close to the micelle-water interface where escape of the photoproduced ions is most favorable. It is therefore suggested that quenching of the P/DMA exciplex by collision with the water pools does not lead to a separation of its constituent radical ions.

In CTAB-μE systems containing small water pools (W_0 = 20.3), the decay of the absorption of the anion of the pyrene derivatives (monitored at 493 nm) manifests itself in two fractions, a fast decay component (half-life 100 ns) attributed to first-order intra-water pool back ET reaction involving pairs of (P^-, DMA^+) residing in isolated water pools, and a slow second-order decay (half-life 2-3 μs) corresponding to an inter-WP back ET process.

Upon increasing the concentration of water in the μE system (W_0 = 60.9) the decay of P^- absorption no longer shows a distinct two-component feature but it remains nonexponential with a half-life of 2-3 μs. In the present μE system which contains larger water pools (see Table IV), the intra-WP back ET process is projected to occur within a few μs and therefore would be mixed in with the second-order inter-WP reaction which occurs within a comparable time period.

RuII/MV^{2+}/HV^{2+}. The laser flash photolysis technique was also applied to investigate the ET from photoexcited RuII to MV^{2+}, a reaction which is expected to take place inside the water pool, and to HV^{2+} which as indicated earlier is probably located at the interface boundary as a result of its amphiphilic structure. Results showed no yield of MV^+ (monitored at 395 nm) ions presumably due to a very fast back ET to RuIII, but a high yield of HV^+. The transient absorption of HV^+ decayed by two processes (similar to the case of P/DMA discussed above) intra- and inter-WP back ET reaction occuring in a time range of ca. 10 μs.

Attempts to intercept the back transfer of the electron from MV^+ to RuIII by addition of EDTA which would react with RuIII to regenerate RuII turned out not to be successful. However, in the case of RuII/HV^{2+} addition of EDTA increased the lifetime of HV^+ by more than an order of magnitude.

Conclusions

The data establish several important parameters such as water pool radius and hydrocarbon bubble radius for cationic W/O and O/W CTAB microemulsions, respectively. Photoinduced reactions, in particular electron-transfer reactions, point out the important role played by environment in controlling the nature of these reactions. Design of the microemulsion system provides factors that control the efficiency of electron transfer and the subsequent efficient separation of the ionic products. The data point out salient features to be obtained for optimum design of electron-transfer systems of interest to solar energy storage.

Highly Conducting Linear Stacked Polymers: Iodine-Doped Fluoroaluminum and Fluorogallium Phthalocyanines

Ronald S. Nohr,[1a] Paul M. Kuznesof,[1b] Kenneth J. Wynne,*[1c] Malcolm E. Kenney,[1d] and P. G. Siebenman[1e]

Contribution from The Chemistry Division, Naval Research Laboratory, Washington, DC 20375, and Department of Chemistry, Case Western Reserve University, Cleveland, Ohio 44106.
Received April 21, 1980. Revised Manuscript Received February 5, 1981

Abstract: Phthalocyanine-aluminum and phthalocyanine-gallium fluorides have been prepared and doped with iodine to give $(PcMFI_x)_n$ compositions, where x = 0.012-3.4 (M = Al) and x = 0.048-2.1 (M = Ga). Thermogravimetric analysis proved useful for iodine analysis as complete loss of I_2 is observed for these materials below 250 °C, leaving a PcMF residue. Both Raman and infrared spectroscopy were used to characterize the iodine-doped PcMF materials. The Raman spectra (ν_0 = 514.5 nm) of $(PcMFI_x)_n$ showed strong scattering attributable to I_3^- (106-108 cm^{-1}) and I_5^- (164-168 cm^{-1}). The pentaiodide band dominated the spectra of all samples with the exception of compositions prepared by heating $(PcAlFI_{3.4})_n$ to temperatures less than 200 °C for which the 107 cm^{-1} (I_3^-) transition was strongest. Conductivity of iodine-doped materials was studied by using linear four-probe (300 K) and variable temperature (77-300 K) van der Pauw methods on pressed pellets. Iodine doping results in increases in conductivity by factors as high as 10^9, with the highest conductivity (5 Ω^{-1} cm^{-1}) being observed for $(PcAlFI_{3.4})_n$ derived from sublimed $(PcAlF)_n$. The conductivity is thermally activated, with an apparent activation energy of 0.017 eV being measured for $(PcAlFI_{3.4})_n$.

Conducting and photoconducting organic and inorganic materials are of considerable interest as new candidates for optical, electronic, photoelectric, and electrochemical applications.[2] Because of their thermal and hydrolytic stability, intense color, and ready availability, phthalocyanines[3] have been the subject of study with regard to their photoconducting and semiconducting properties. Highly conducting doped phthalocyanines have been prepared,[4] and for one composition, $NiPcI_{1.0}$,[5] metallic behavior

0002-7863/81/1503-4371$01.25/0